DOI: 10.1002/cmdc.200600262

Immunostimulatory CpG Oligonucleotides Form Defined Three-Dimensional Structures: Results from an NMR Study

Guangyu He,[a, c] Amritraj Patra,[a] Karsten Siegmund,[a] Mirjam Peter,[b] Klaus Heeg,[b] Alexander Dalpke,[b] and Clemens Richert*[a]

The DNA eicosamer 5′-TCCATGACGTTCCTGATGCT-3′ is known to stimulate the innate immune system of vertebrae. The immunostimulatory activity is based on the activation of Toll-like receptor 9 (TLR9). While it is known that the CG dinucleotide of the eicosamer has to be unmethylated, the structural basis of the recognition of the DNA through the receptor remains unclear. Oligodeoxynucleotides containing the sequence of the eicosamer, or a portion thereof, ranging in length from hexamer to pentaeicosamer were studied by ^{1}H NMR spectroscopy. Based on two-dimensional NMR spectra, a number of resonances could be unambiguously assigned. For all oligonucleotides, structural transitions were detected upon heating, as monitored by the line width and chemical shift of low-field resonances. This includes the TC dinucleotide of the 5′-terminal portion, which does not have any clear base-pairing partners. The melting transitions, together with the NOESY cross-peaks, demonstrate that structure formation occurs well beyond the core hexamer 5′-GACGTT-3′, a fact that may be important for understanding the molecular recognition by the Toll-like receptors of the innate immune system.

Introduction

Oligodeoxynucleotide sequences with unmethylated deoxycytidine residues in the dinucleotide motif 5′-CG-3′ can stimulate the innate immune system of vertebrae.[1,2] This effect was first observed for bacterial DNA,[3] and was later demonstrated in detail with phosphorothioates, a class of compounds employed for antisense inhibition of gene expression.[4] Cells of the innate immune system, upon sensing "CpG oligonucleotides", release cytokines and chemokines, leading to proinflammatory responses.[5,6] The immunostimulatory effect is being explored for therapeutic applications ranging from vaccination[7] to the treatment of infections,[8] allergic diseases and cancer, and several oligodeoxynucleotides have entered clinical or pre-clinical trials.[9] For example, CpG oligonucleotides are used as adjuvants for vaccination against hepatitis B surface antigen, HIV, and *Trypanosoma*, and may be developed to bias immune responses towards a preferential T_h1 response[10] to prevent allergic disorders in humans.

The molecular recognition of CpG oligonucleotides by the cells of the innate immune system involves membrane-bound proteins of the family of Toll-like receptors (TLRs).[11,12] These membrane-bound receptors then initiate an intracellular signaling cascade.[13,14] Toll-like receptor 9 (TLR9) induces an immune response to synthetic oligodeoxynucleotides,[15] and direct interactions between the DNA and the receptor have been demonstrated.[16,17] Two X-ray crystal structures of the extracellular domain of TLR3, a related receptor that binds double-stranded RNA, have been published,[18,19] revealing a horseshoe-like shape of the leucine-rich repeats, but the crystals did not contain ligands. How the TLRs recognize DNA is not known. In a discussion of the specificity of key TLRs (TLR 3, 7, 8, and 9), a recent review on Toll-like receptors states that "the polyanionic nature of nucleic acids […] presents problems for specific recognition. It is unclear how specificity of the kind shown by intracellular nucleic-acid-binding proteins, such as transcription factors, can be achieved."[20]

It is known that the binding of fully complementary strands to CpG oligonucleotides lowers their immunostimulatory activity.[21] This has been interpreted as a sign that the oligonucleotides must be single-stranded to be active.[22] Also, based on experiments involving immunostimulatory oligonucleotides alone, duplexes between the same oligonucleotides and fully complementary DNA strands, or plasmid DNA, it was postulated that the recognition of CpG oligonucleotides by TLRs involves single-stranded DNA and not double-stranded DNA.[17]

[a] *G. He,[+] A. Patra,[+] Dr. K. Siegmund, Prof. C. Richert*
Institute of Organic Chemistry, University of Karlsruhe (TH)
Fritz-Haber-Weg 6, 76131 Karlsruhe (Germany)
Fax: (+49) 721-608-4825
E-mail: cr@rrg.uka.de

[b] *M. Peter, Prof. K. Heeg, Prof. A. Dalpke*
Department of Medical Microbiology and Hygiene, University of Heidelberg
Im Neuenheimer Feld 324, 69120 Heidelberg (Germany)

[c] *G. He[+]*
Current address:
Key Laboratory of fine Chemical Engineering, Jiangsu Polytechnic University
Changzhou, 213016 (China)

[+] *These authors contributed equally to this manuscript.*

Supporting information for this article is available on the WWW under http://www.chemmedchem.org or from the author.

Current models of receptor binding continue to depict the DNA in single-stranded form.[23] However, no direct evidence for the absence of double-stranded helical regions in the recognized DNA has been provided. One report suggests the formation of secondary structures, but again, hairpin-type intramolecular folding is proposed (based on prediction algorithms), and not intermolecular duplex formation.[24]

It is known that the sequence flanking the unmethylated CpG motif matters. The sequence motif PuPuCGPyPy (Pu = purine, Py = pyrimidine) is highly active in mice, whereas PuTCGPyPy is highly active in primates.[25,26] Prominent among the hexamer sequences are those in which the self-complementary CG dinucleotide is surrounded by nucleotides that can form A:T or G:T (wobble) base pairs in antiparallel duplexes. Furthermore, it is known that structural modifications at the 5′ terminus are less well tolerated than modifications at the 3′ terminus,[27] leading to the development of "immunomers", that is, 3′–3′-linked dimers[28] of oligonucleotides.[29]

Selectivity in molecular recognition is important for the immune system, as incorrect recognition can cause autoimmune diseases or uncontrolled proliferation of infections. The innate immune system, with its pattern-recognition receptors, is believed to show almost perfect selectivity, so that it never recognizes host structures.[30] On a molecular level, this selectivity must be based on the recognition of specific molecular structures with exquisite selectivity. For biomacromolecules such as proteins and nucleic acids, folding into secondary, tertiary, and possibly quaternary structures greatly affects (and often dictates) recognition in the cell. Binding such a defined three-dimensional structure selectively is generally easier than binding a flexible unfolded oligomer, as structural diversity can be more readily realized in three dimensions than in two. Furthermore, binding tightly to a folded biomacromolecule is more favorable on thermodynamic grounds than binding to a flexible structure, as the entropy loss upon complex formation is much decreased (Figure 1).

Even functional oligoribonucleotides of modest length, such as tRNAs, are recognized by their cognate enzymes (for example, aminoacyl tRNases and binding partners of the ribosomal machinery) in a folded state,[31] not in single-stranded state. Moreover, there are very few proteins that bind single-stranded DNA in a sequence-selective manner, whereas proteins that bind duplex DNA abound in cells, and the genes encoding them can make up a large portion of entire genomes.[32] Thus, receptors that bind double-stranded DNA may have been readily developed during evolution through gene duplication and mutagenesis.

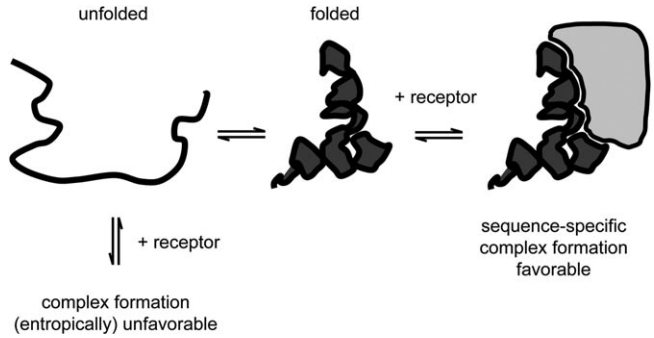

Figure 1. A depiction of the role of defined three-dimensional structures in the selective recognition of biomacromolecules. Receptors that bind biomacromolecules, including those that form nucleic acid–protein and protein–protein complexes in a sequence-specific manner, usually bind a folded structure, not the random-coil state.

Consequently, it would seem that the recognition of a folded (duplex-containing) structure by TLR9 is more likely to occur than the selective recognition of an entirely unstructured, random-coil oligomer. The core recognition motif found in immunostimulatory oligonucleotides is the dinucleotide 5′-CG-3′, which is also the very dinucleotide known to form the most stable duplex among all 16 dinucleotide sequences possible.[33] Additionally, the molecular label that differentiates bacterial DNA from mammalian DNA recognized by TLR9 is a methyl group at position 5 of cytosine, that is, a position in the major groove of duplexes, where the probe helices of sequence-specific binding proteins are known to reside.[34]

An isolated dinucleotide alone is, of course, insufficient to induce formation of a stable duplex, though it should suffice to bias a binding equilibrium significantly. Sequence motifs known to be immunostimulatory in humans often contain several CG dinucleotides[26,35] that together may lead to sufficient duplex strength. Also, as mentioned above, sequences that stimulate cells of the innate immune system often contain flanking nucleotides that favor duplex formation. This includes the sequence TCGTTTTTTTTTTTT, which shows slightly lower activity than the sequence TCGAAATTTTTTTTTA, whose 5′-terminal tetramer is fully complementary.[36] Given this situation, it is surprising that there appear to be no systematic studies on the propensity of immunostimulatory sequences to form defined three-dimensional structures. This may be due, in part, to the extensive use of phosphorothioates in medically oriented studies. Phosphorothioates have a modest duplex-destabilizing effect, but often achieve higher activity in vivo through increased resistance to nuclease degradation and/or altered biodistribution pathways.

We have shown previously that the best-known sequence motif for immunostimulation of murine cells can indeed form duplexes.[37] We observed that CpG oligonucleotides with linkers that favor nicked duplex structures are highly active, whereas N3-methylated thymidine residues that interfere with duplex formation decrease immunostimulatory activity.[37] More recently, a systematic study by Agrawal and colleagues involving mouse, monkey, and human systems came to the conclusion that a sequence that forms a duplex is required for IFN-α induction, and that a stable secondary structure induced the highest levels of IFN-α.[38] No experimental data confirming the designed structures was provided, however. Herein we present results from an NMR spectroscopic study that demonstrates structure formation beyond a simple duplex for the well-characterized immunostimulatory DNA eicosamer sequence motif initially described by Krieg and colleagues in their seminal paper.[39]

Results

The oligonucleotides studied in this work are shown in Figure 2. They include eicosamer **1**, known for its immunostimulatory activity toward cells of the murine innate immune

GACGTT (3)
6 7 8 9 10 11

ATGACGTTCC (4)
4 5 6 7 8 9 10 11 12 13

CCATGACGTTCCTG (5)
2 3 4 5 6 7 8 9 10 11 12 13 14 15

TCCATGACGTTCCTGATGCT (1)
1 2 3 4 5 6 7 8 9 10 11 12 13 14 15 16 17 18 19 20

TCCATGACGTTCCTGATGCTGGGGG (2)
1 2 3 4 5 6 7 8 9 10 11 12 13 14 15 16 17 18 19 20 21 22 23 24 25

Figure 2. DNA sequences employed in the work reported herein with residue numbering in gray beneath each nucleotide letter. All sequences are shown oriented 5′ to 3′ terminus.

system.[15,25,39] It is well established that both the natural phosphodiester version of **1** and its phosphorothioate version are active immunostimulatory compounds.[37,39] Phosphorothioates are not suitable for high-resolution structural studies, though, because they are formed as mixtures of diastereomers. Included in our study was pentaeicosamer **2**, whose pentameric deoxyguanosine 3′ tail enhances the immunostimulatory activity of **1**,[40] most likely because of improved cellular uptake.[24] Furthermore, hexamer **3**, decamer **4**, and tetradecamer **5** were included as shorter versions of **1**, as their NMR spectra are less complex. We decided to use the residue numbering of **1** for all oligonucleotides studied to simplify the discussion of our results.

Low-resolution three-dimensional structure of $(3)_2$

In our earlier work, we had been able to show that immunostimulatory eicosamer **1** gives a melting transition in UV-monitored thermal denaturation experiments,[37] suggesting that this compound does not occur as a simple random-coil oligomer, but engages in structure formation. Because the melting point for **1** increases with concentration,[37] it was clear that the melting transition is caused by *inter*molecular complex formation, not *intra*molecular folding. This finding clarified earlier proposals based on theoretical modeling that suggested a stem–loop structure.[41a] We suspected that antiparallel Watson–Crick duplexes form, with base pairing in the region of the core hexamer 5′-GACGTT-3′.[37] This hypothesis was corroborated by the fact that the hyperchromicity accompanying thermal denaturation of the complex formed by **1** was smaller than expected for a duplex stretching along the entire length of the eicosamer. Also, exploratory NMR work on the core hexamer **3** provided inter-residue NOESY cross-peaks consistent with duplex formation.[37]

Based on additional one- and two-dimensional NMR work, we have now calculated a low-resolution three-dimensional structure of $(\mathbf{3})_2$. For this, NOE-based distance constraints from a NOESY spectrum were used to perform restrained molecular dynamics calculations. The available number of constraints for this very short helix is insufficient to allow the generation of a high-resolution structure, but an overlay of the low-energy structures obtained from our calculations (Figure 3a) clearly shows a duplex. Imino resonances characteristic for duplex formation were observed for the correct number of Watson–Crick base pairs (Figure S2, Supporting Information). Furthermore, there are NOESY cross-peaks between the amino group at position 4 of C3 and H1 of G4 at mixing times of 70, 130, and 250 ms, providing direct proof for a duplex with C:G base pairs. As expected, we did not observe the imino resonances of terminal G:T wobble base pairs, which are exposed to solvent, but the number of constraints to G6 and T11 is sufficient to localize them in a geometry that is consistent with a wobble base pair (Figure 3b).

Thermal denaturation of $(3)_2$

It is known that the non-exchangeable protons of the nucleotides of DNA duplexes exhibit exchange broadening in the vicinity of the midpoint of the melting transition.[42] The extent

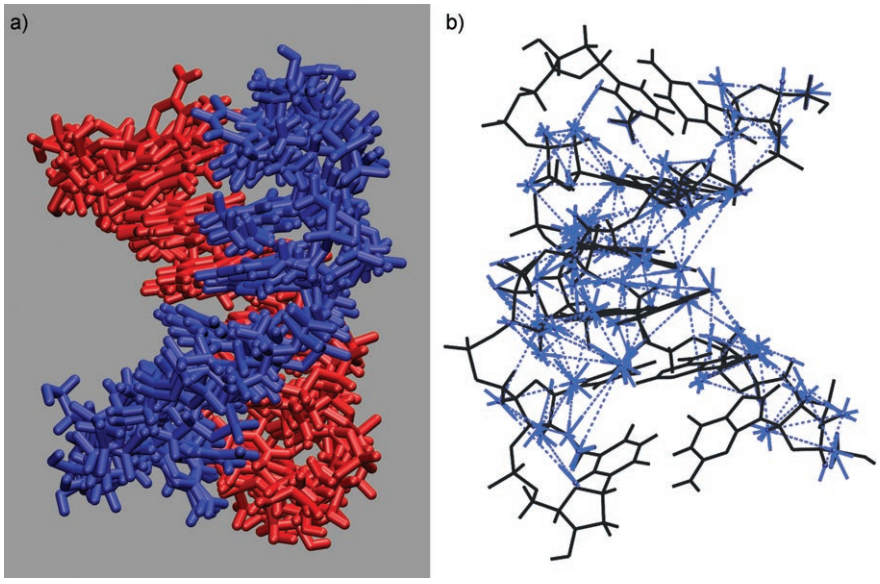

Figure 3. Low-resolution structure of $(GACGTT)_2$, as obtained by restrained molecular dynamics; a) overlay of low-energy structures; b) representative low-energy structure with distance constraints displayed as dotted blue lines and boundaries of constraints shown as solid blue lines. See Table S4, Supporting Information for further details.

of broadening for a given resonance depends on the chemical shift difference between the duplex and single-stranded states.[43] Thus, the absence of distinct broadening does not necessarily mean that no transition occurs, but simply that the chemical shifts for the given resonance are (incidentally) similar for the two states. For protons where the chemical shift differences are significant, the maximum line width may be observed at a temperature below the melting point determined by chemical shift or UV-melting analysis.[43] We interrogated local transitions in the DNA structures studied by plotting the line width against temperature. Duplex dissociation was thus confirmed for $(\mathbf{3})_2$ from a series of one-dimensional ^{1}H NMR spectra acquired at temperature intervals of 10 °C (Figure 4).

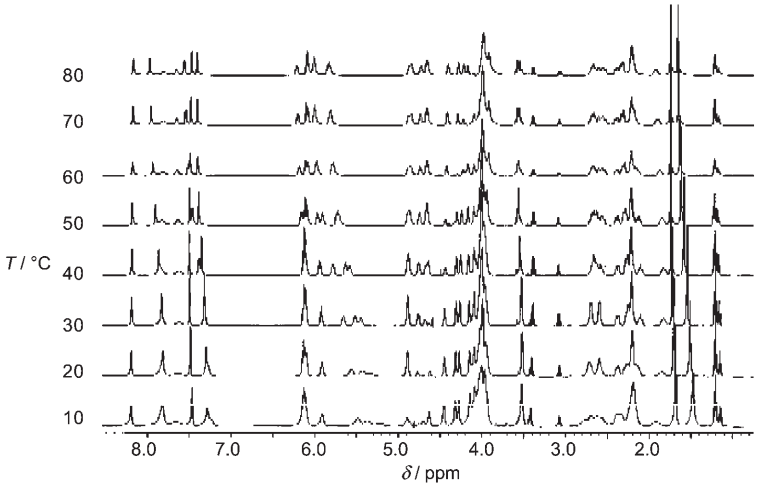

Figure 4. Duplex dissociation of $(\mathbf{3})_2$ as monitored by a series of ^{1}H NMR spectra acquired from 10 to 80 °C in increments of 10 °C.

Upon heating, the broad signals sharpened again, and the large $\Delta\delta$ spread of the H1′ and H5 resonances (5.0–6.3 ppm), typical of duplexes, disappeared, consistent with the transition to a single-stranded, random-coil conformation. The transition to the single-stranded form, as monitored by line broadening, was essentially complete at 50 °C, and changes in chemical shift were modest beyond this temperature.

Immunostimulatory activity of 1 and shortened versions thereof

Since full NMR assignment seemed unrealistic for eicosamer **1** with natural isotope abundance, we employed truncated versions **4** and **5** in our structural work. Before doing so, we wished to know to what extent the decamer and tetradecamer retain the immunostimulatory activity of parent compound **1**, hoping to demonstrate that we were using compounds relevant for the molecular recognition by the receptor(s) we were interested in. Figure 5 shows the results from ELISA assays detecting tumor necrosis factor α (TNFα) in the supernatant of murine macrophages previously stimulated with **1**, **4**, **5**, or the phosphorothioate analogue of **1** (1668-PS).[39]

Under these conditions, all four compounds showed immunostimulatory activity at submicromolar concentrations. The activity decreased with decreasing length of the phosphodiester compounds, but the overall appearance of the dose–response curves was similar for **1**, **4**, and **5**. The phosphorothioate gave a flatter curve than **1**, in agreement with earlier results.[37] Decamer **4** required the presence of the transfection agent DOTAP[44] to give significant activity, and tetradecamer **5** was also less active without it, as determined in assays in the absence of this agent (Figure S1, Supporting Information). This suggests that the uptake of the shortened versions of **1** is less efficient than that of the parent compound. Preliminary results from a reporter system with cell-surface-expressed TLR9[45] show activity for compounds **1**, **4**, and **5** in the absence of DOTAP.

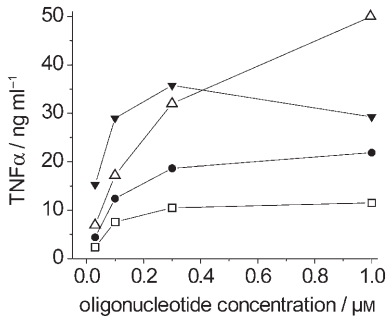

Figure 5. Dose–response curves for the immunostimulation of cultured RAW 264.7 macrophages with synthetic oligodeoxynucleotides in the presence of DOTAP as transfection agent, as measured through the release of TNFα. Besides decamer **4** (□), tetradecamer **5** (●), and eicosamer **1** (△), the phosphorothioate version of **1** (1668-PS; ▼)[39] was included as positive control. Data points represent the average of two independent experiments. Background without oligodeoxynucleotide < 0.1 ng mL^{-1} (no measurable TNF secretion). See Figure S1, Supporting Information for results obtained without DOTAP.

NMR study of decamer 4

The ^{1}H NMR data obtained for decamer **4** in phosphate-buffered solution show signs of duplex formation. There are three resonances in the low-field region (Figure 6a), indicative of three hydrogen-bonded protons sufficiently shielded to avoid fast exchange with the solvent. Two of these are in a range typical for imino protons engaged in Watson–Crick base pairing (11–14 ppm).[46] Furthermore, a NOESY spectrum acquired at 14 °C showed a cross-peak pattern consistent with the formation of a duplex (Figure 7).

These cross-peaks allowed resonance assignment of all H1′ and nucleobase protons by conventional NOESY-based methods for DNA duplexes.[46] The starting point for the assignment was the H6 resonance of C8, which was identified on the basis of the DQF-COSY cross-peak to its H5 neighbor and a characteristic pattern of cross-peaks to the neighboring purine residues. This starting point provided an entry into sequential assignments of all H1′ and H8/H6 resonances.[46] Only the cross-peak between H1′ of C12 and H6 of C13 (terminal deoxycytidine residue) is missing. Due to severe peak overlap, few H4′

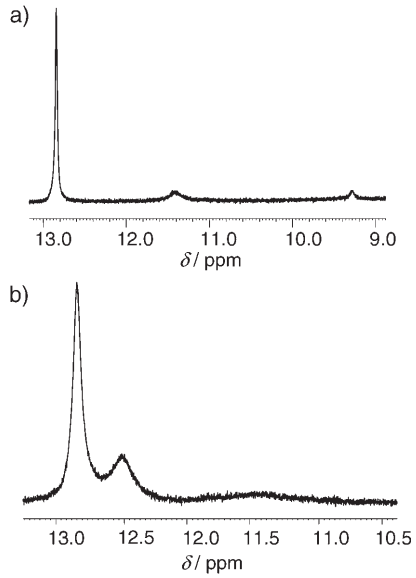

Figure 6. Low-field region of the WATERGATE ^{1}H NMR spectra containing the imino proton resonances of oligonucleotides at 5 °C in phosphate-buffered saline, D_2O/H_2O (1:9, *v/v*): a) decamer **4**; b) eicosamer **1**.

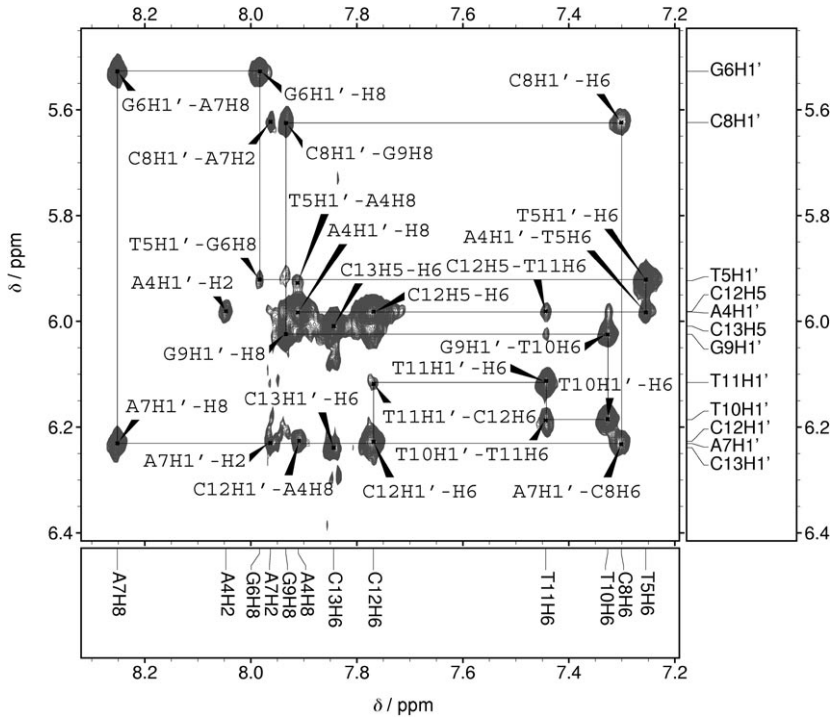

Figure 7. Expansion of the NOESY spectrum of **4** in D_2O/phosphate-buffered saline at 14 °C showing cross-peaks between nucleobase and deoxyribose resonances. Assignments are given next to cross-peaks and on the axes. The thin lines connecting cross-peaks highlight the sequential connectivity between H1′ and nucleobase resonances used to assign nucleotides in the chain.

and H5′/H5′′ resonances could be assigned, whereas most other protons of the deoxyribose spin systems were identified based on cross-peaks in COSY, TOCSY, and NOESY spectra. The assignments were checked for consistency and were confirmed by an alternative assignment strategy involving cross-peaks between base protons and H2′ and H2′′ resonances. A list of chemical shifts of key resonances is given in Table S2 of the Supporting Information.

We next studied thermal denaturation of the structure formed by **4**. A plot of the low-field region of the one-dimensional ^{1}H NMR spectra at different temperatures is shown in Figure 8. It is clear from chemical shift changes and from changes in peak widths that a structural transition occurs in the decamer. Importantly, this transition affects more than just the six residues of the core hexamer GACGTT. The assignment of the low-temperature form based on the 2D spectra is shown in the lower part of Figure 8, and the proposed assignment of the high-temperature form is given above the spectrum acquired at 90 °C. Tracing the signals was facilitated by two-dimensional spectra acquired at 34 °C. Some uncertainties remain concerning the assignment of A4H8, G6H8, and G9H8 at elevated temperature because of the peak overlap and broadening between 16 and 32 °C, but the line-width changes are so similar that all three were classified as ordered at low temperature.

A plot of line width against temperature (Figure 9) confirms what is suggested by the chemical shift changes visible in ^{1}H NMR melting curves, namely that at least seven of the residues undergo a transition from one state to another upon heating. A sigmoidal melting transition can also be readily discerned in separate plots of chemical shifts versus temperature (Figure S4, Supporting Information). Only the H6 resonance of the 3′-terminal residue C13 shows neither a significant change in chemical shift ($\Delta\delta =$ 0.02 ppm between 10 and 90 °C) nor substantial exchange broadening upon heating the low-temperature form. This most likely reflects the fact that this residue dangles freely in the solvent. The low-field resonances of the two residues flanking the core hexamer (T5 and C12) are broader at low temperature than that of C13, reaching values similar to those of the resonances of the core hexamer, but again no distinct maximum in the plot of line width versus temperature is observed. Still, the chemical shift change upon heating, particularly for H6 of T5, is significant enough to suggest some stacking interactions with the ordered part of the sequence.

Whereas the sign of the chemical shift change differs for the downfield resonances of the core hexamer, the maximum in the line-width plot (Figure 9a) induced by exchange broadening is very similar for these resonances. This suggests that this

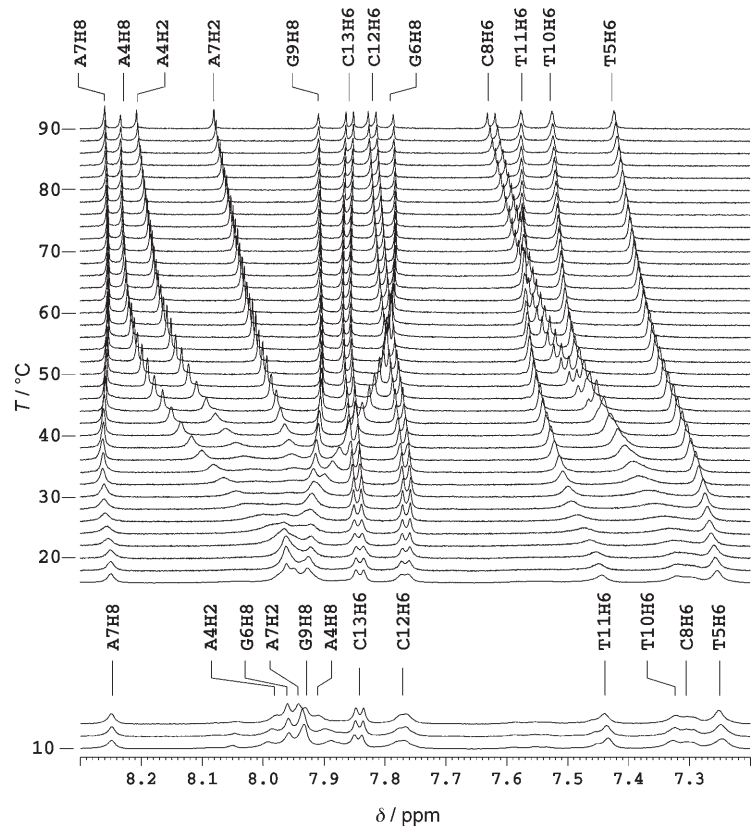

Figure 8. Thermal denaturation of the structure formed by **4**, as monitored by a series of ^{1}H NMR spectra acquired at temperatures between 10 and 90 °C. The region containing the resonances of protons from the nucleobases is shown, together with assignments at low temperature (above the spectrum acquired at 14 °C) and at high temperature (above the spectrum acquired at 90 °C).

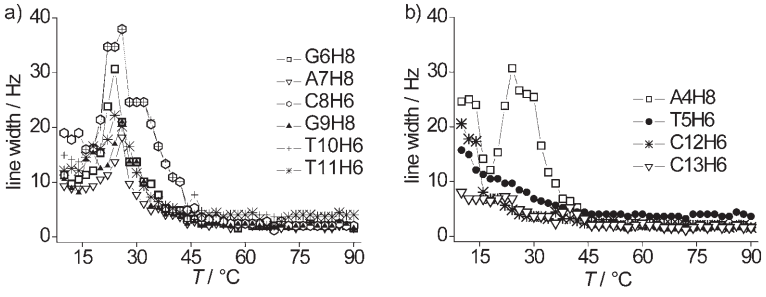

Figure 9. Duplex dissociation of $(\mathbf{4})_2$ traced from 10 to 90 °C in increments of 2 °C by line widths of selected protons from nucleobases; a) the line-width changes of the core hexamer portion (G6–T11) of **4** are similar; b) the line-width change of A4H8 is different from all the others.

core portion of **4** forms a duplex structure that melts cooperatively. As expected,[43] the maximum in broadening occurs at a temperature below the midpoint of the transition visible by following chemical shift changes (Figure 8), so a "softening" of the structure sets in before the strands fully dissociate. This and the sequential NOESY cross-peak pattern observed for all but the 3′-terminal residue of **4**, strongly suggest that the core hexamer forms a duplex similar to that of **3**.

The greatest surprise of the NMR study on **4** was the strong change in chemical shifts and pronounced line-width changes for resonances of A4 at the 5′ terminus of the decamer. The resonances of H8 as well as that of H2 of this residue show exchange broadening at intermediate temperatures (Figure 9b) and massive chemical shift changes upon heating. Furthermore, at 14 °C, a number of NOESY cross-peaks were observed between protons of A4 and T11, the residue believed to form the terminal wobble base pair of the core duplex. Because A4 seems to lack a base-pairing partner, this suggests that at lower temperature, this 5′-terminal adenosine residue folds back onto the core duplex.

NMR study of tetradecamer 5

The NOESY spectrum of tetradecamer **5** (Figure 10) again showed a pattern of cross-peaks indicative of the formation of a defined three-dimensional structure. This allowed assignment of the resonances following the principles mentioned. The sequences of H6/H8→H1′ internucleotide cross-peaks are interrupted between C2 and C3, as well as those between C12 and C13, owing to peak overlap. Combining the remaining connectivity information with that of a sequential analysis based on H6/H8→H3′ cross-peaks still gave an unambiguous result.

Based on the assignment at 10 °C and additional spectra acquired at 30 °C, the pre-melting exchange broadening that accompanies the transition from the ordered to the random-coil form of **5** could be monitored residue-specifically (Figure 12). All residues of the tetradecamer show substantial broadening at low temperature. Moreover, sigmoidal melting transitions are observed for the chemical shifts (Figure 11 and Figure S5, Supporting Information). The main melting transition accompanied by a line-width maximum sets in at around 20 °C and occurs up to approximately 50–60 °C. For some resonances, such as that for H8 of A4, the line width does not go through a maximum, but decreases steadily with temperature. Based on the plots of line widths and the NOESY cross-peaks, there is little doubt that the core hexamer GACGTT is again in duplex form at low temperature.

The line-width change with temperature for G9H8 shows softening of the structure at a slightly lower temperature than for other residues of the core hexamer, but cross-peaks in a NOESY spectrum acquired in H_2O/D_2O show that G9 is engaged in hydrogen bonding to C8 (data not shown). Interestingly, the line-width change for H6 of 5′-terminal C2 as a function of temperature is substantial, and the maximum in peak width is at a similar temperature as those for residues of the core hexamer. The transition in the chemical shift and line width for H8 of G15, the 3′-terminal residue, while clearly present, is not very characteristic, so it is unclear whether both termini loop back toward the core or engage solely in interactions between themselves. A Watson–

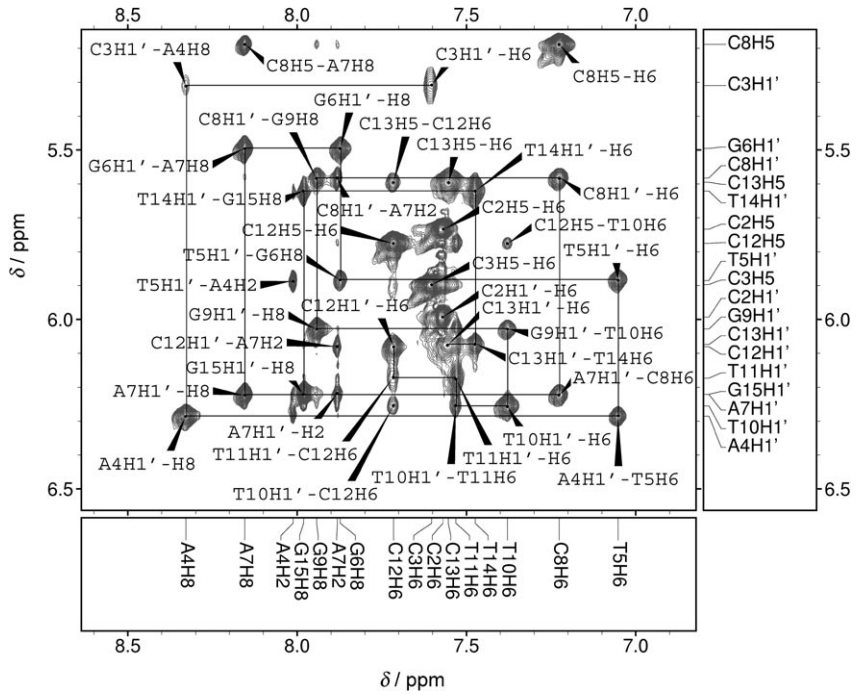

Figure 10. Expansion of NOESY spectrum of **5** in D_2O/phosphate-buffered saline at 10 °C showing cross-peaks between nucleobase and deoxyribose resonances. Assignments are given next to cross-peaks and on the axes. Thin lines connecting cross-peaks show the sequential connectivity between H1′ and nucleobase resonances.

Crick-paired dimer duplex between C3A4 and T14G15 cannot be ruled out.

NMR study of eicosamer 1 and pentaeicosamer 2

Encouraged by the results with model compounds **4** and **5**, we then performed exploratory work with eicosamer **1** and pentaeicosamer **2**. Figure 6b shows the imino resonances of **1** detectable by ^{1}H NMR spectroscopy with the WATERGATE pulse sequence[47] in H_2O/D_2O (9:1 *v/v*) at 5 °C. The number of resonances is the same as that observed for **4** (Figure 6a), but the signals are broader and all but the most prominent are shifted to lower field, as expected for tighter hydrogen bonding. For **2**, the imino signals were, in fact, too broad to be readily detectable at a temperature this low. At 40 °C, a sample of **2** in H_2O/D_2O (9:1 *v/v*) shows five peaks between 10 and 12 ppm, suggesting extensive hydrogen bonding interactions (Figure S3, Supporting Information).

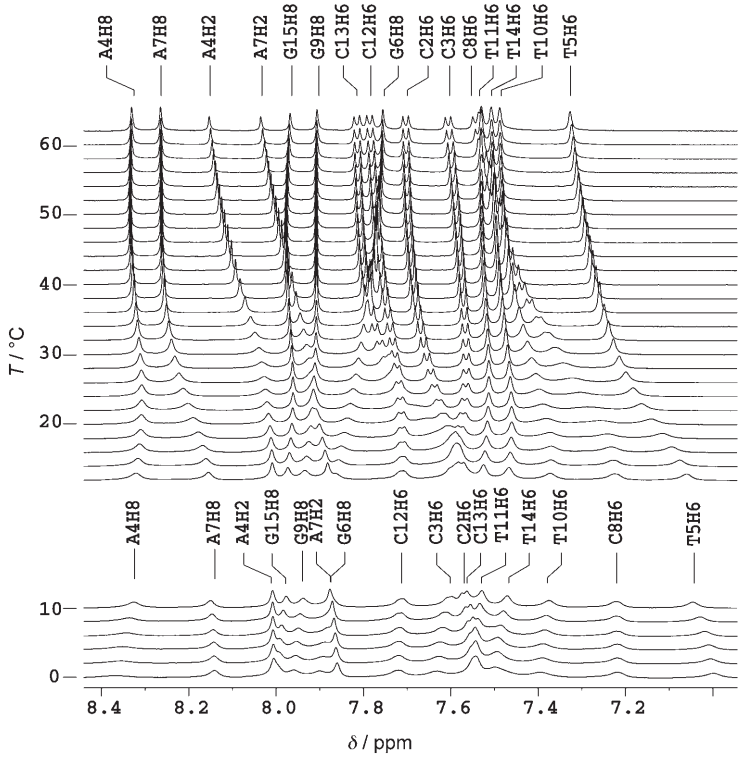

Figure 11. Thermal denaturation of the structure formed by **5** as monitored by ^{1}H NMR. The low-field region containing the resonances of protons from the nucleobases is shown for spectra acquired between 0 and 62 °C. The assignment is considered unambiguous and is indicated at high temperature.

We acquired a set of two-dimensional NMR spectra of **1** in D_2O at 20 °C, as a compromise between decreasing line widths and increasing dynamics. Based on this data, complemented with NOESY spectra acquired at 10 °C either in D_2O or H_2O/D_2O, a tentative assignment was carried out (Figure 13). Due to peak overlap, the assignment must be considered "very tentative" for six nucleotides in the 3′-terminal region (C12–G15 and C19/T20). Based on cross-peaks in the NOESY spectrum acquired in H_2O/D_2O, it could be demonstrated that G9 forms hydrogen bonds with C8, and that A7 is base-paired with T10 (compare Figure S6, Supporting Information). This confirms that the central tetramer of the GACGTT core indeed forms a duplex.

A series of one-dimensional proton NMR spectra was acquired for **1** to follow the transition from duplex to the random-coil state. The NMR results are complemented by melting-curve-derived thermodynamic data (Table 1). The NMR "melting curves" are shown in Figure 14. Again, it is clear that a structural transition sets in at approximately 20 °C and continues at least up to 50 °C. Line broadening and chemical shift changes at low temperature occur to a different extent for different residues of the eicosamer. There is no doubt, however, that the 5′-terminal region, up to T1, is involved in a structural transition.

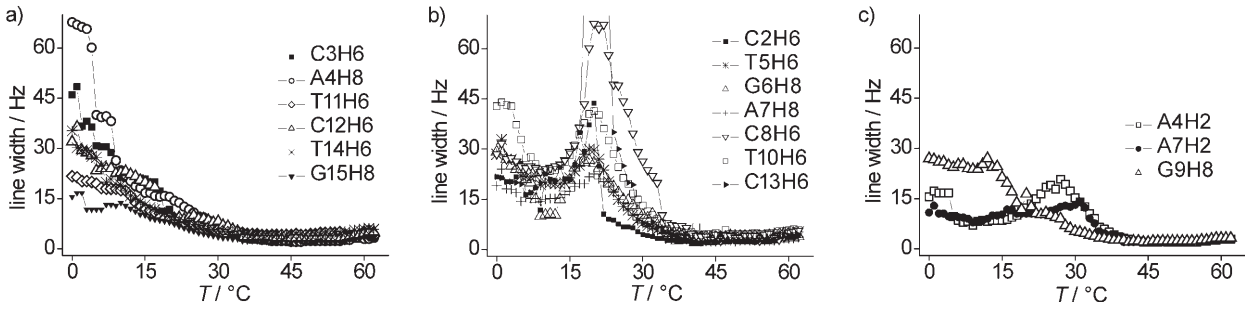

Figure 12. Denaturation of the structure formed by **5**, as traced from 0 to 62 °C by exchange-broadening-induced line-width changes of selected protons of nucleobases.

Table 1. Thermodynamic parameters of duplex formation for oligonucleotides **1** and **4**.[a]

Oligonucleotide	ΔH [kcal mol^{-1}]	ΔS [cal K^{-1} mol^{-1}]	ΔG [kcal mol^{-1}]	T_m [°C][b]
1	33.1 ± 2.4	86 ± 9	6.5 ± 0.2	44.8
4	37.6 ± 2.2	109 ± 7	3.7 ± 0.1	21.6

[a] Average values ± SD determined from four experimental UV-melting curves at a strand concentration of 2.9 or 64 μM. [b] UV-melting point, as calculated by Meltwin[48] for a strand concentration of 0.1 mM, 10 mM phosphate buffer, 150 mM NaCl, pH 7.0.

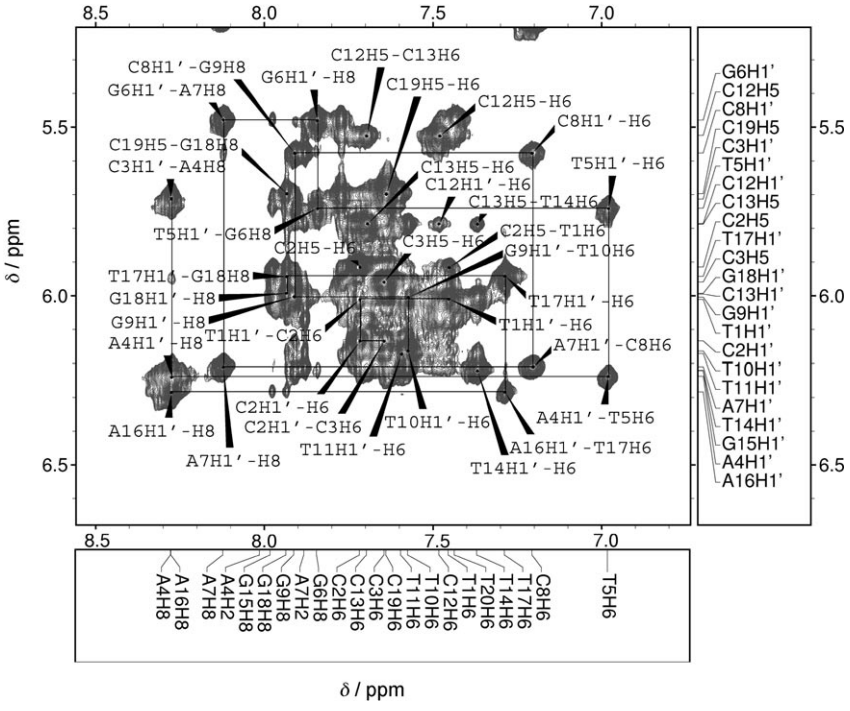

Figure 13. Expansion of a NOESY spectrum of **1** in D_2O/phosphate-buffered saline at 20 °C showing the region with cross-peaks between nucleobase resonances and H1′/H5 resonances. Tentative assignments of cross-peaks and resonances are given on the spectrum and in the margins.

This becomes particularly clear from a plot of line widths versus temperature (Figure 15a) for nucleobase protons of residues T1, T5, and A7. The maximum extent of exchange broadening is reached in a similar temperature range for the thymidine residues in the 5′-terminal region as for the deoxyadenosine group of the core hexamer portion. Since it is unlikely that a completely separate helical region of similar stability can form between 3′- and 5′-terminal flaps around the core hexamer duplex, we take this finding as a sign for direct interactions between the 5′-terminal region and the GACGTT core. The 5′-terminal TC dinucleotide has been described as critical for activity.[23] Further support for duplex-stabilizing interactions between the terminal regions of the eicosamer and the core comes from the increase in melting point relative to the decamer and tetradecamer fragments. Whereas all three compounds (**1**, **4**, and **5**) show a melting point increase with concentration that is characteristic of intermolecular complex formation (Table S3, Supporting Information and Table S1 in the supporting information for reference [36]), the melting point of **4** is approximately 20 °C lower than that of **1** (Table 1), and the melting point of **5** is slightly lower still (Table S3, Supporting Information). Based on the available data (Figure 15b), it is possible, but by no means certain, that portions of the 3′ tail of the eicosamer are part of the structure formed by the remainder of the sequence.

The ^{1}H NMR resonances of pentaeicosamer **2** are too broad to be assigned at a temperature at which complex formation occurs. We have not yet found conditions that would overcome this difficulty. We assume that the additional broadening is due to intermolecular aggregation, which might be caused by the formation of quadruplexes[49] induced by the $d(G)_5$ tail. It is possible that a strict exclusion of potassium and sodium ions would suppress this phenomenon. Thermal denaturation was detected by NMR, however, (Figure 16). Much like the tempera-

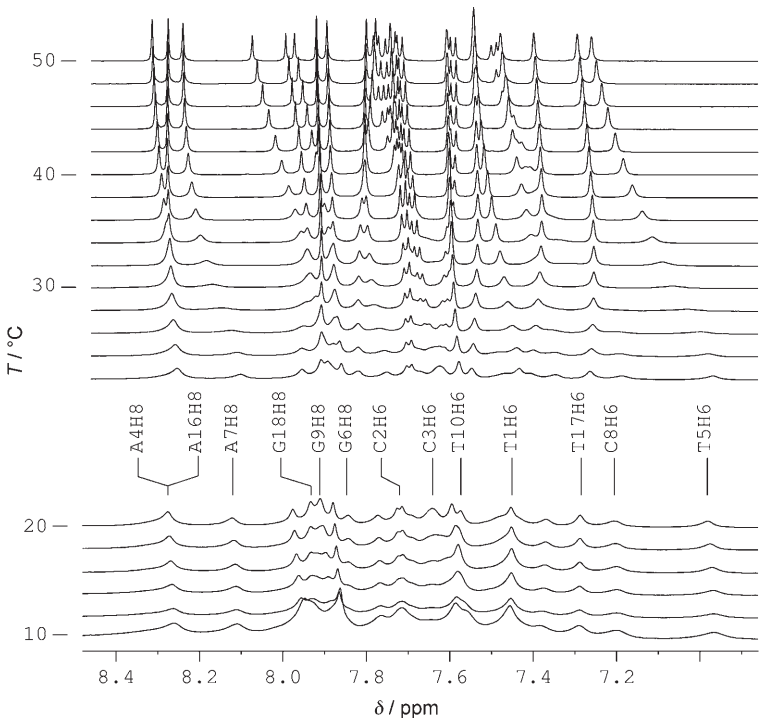

Figure 14. Thermal denaturation of the structure formed by **1** as monitored by a series of ^{1}H NMR spectra acquired from 10 to 50 °C in increments of 2 °C. The region containing the resonances of protons from the nucleobases is shown with selected assignments.

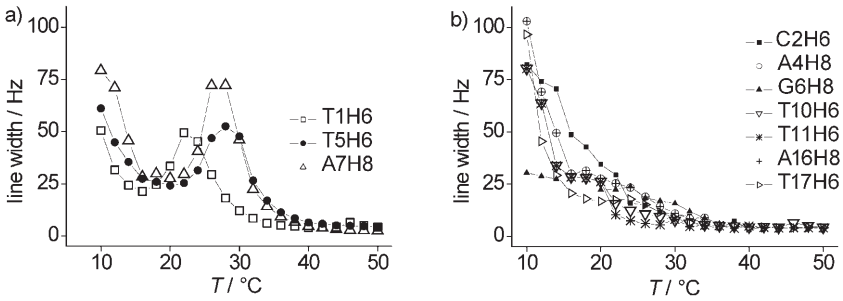

Figure 15. Structural transition in **1** upon heating, as traced by line widths of selected proton resonances from nucleobases whose assignment is considered reliable.

ture series for **1**, the data show that different residues of the sequence are affected by line broadening at low temperature to varying extents. Unlike the eicosamer, the pentaeicosamer continues to show signs of dissociation above 60 °C. Apparently, the $(dG)_5$ tail not only increases the size of the structures formed (leading to slow tumbling and excessive line widths at low temperature), it also seems to stabilize the overall assemblies towards thermal denaturation. This may be of consequence for cellular uptake[50] and molecular recognition.

Discussion

Several conclusions may be drawn from the data presented here. Firstly, eicosamer **1** does not occur as a monomeric random-coil single-stranded structure at or below body temperature at millimolar concentration. Secondly, there is substantial line broadening beyond what can be expected for a simple duplex at low temperature, most probably due to the slow tumbling of larger species in solution. This effect is even stronger for the pentaeicosamer **2** with its oligodeoxyguanosine tail that favors aggregation. The formation of such larger species may be of importance for uptake into cells via endocytosis.[24] It is believed that signaling through TLR9 occurs only after CpG oligonucleotides are taken up via endocytosis.[51,52] Thirdly, there is evidence for the formation of a duplex between the residues of the core hexamer GACGTT throughout the series of oligonucleotides **3**, **4**, **5**, and **1**. For **2**, the available spectroscopic data are not yet sufficient to demonstrate this, but it seems likely. Finally, for **5** and **1**, both termini may engage in complex formation, as they do not show the NMR spectroscopic characteristics of dangling residues. The 3′-terminal deoxycytidine residue C13 of decamer **4**, however, does behave like a dangling residue, suggesting that complex formation is not an unspecific general phenomenon for this type of sequence.

A list of the chemical shifts for selected protons of the low-temperature forms of oligonucleotides **1**, **4**, and **5** is given in Table S2 of the Supporting Information. The chemical shift differences between the respective resonances for the protons decrease toward the core part of the sequence. For H8 of the central deoxyguanosine residues, such as G9 of **4**, **5**, and **1**, there are virtually no chemical shift differences among the three compounds, suggesting that the core part of these three sequences has a similar structure. The chemical shift changes associated with duplex dissociation are also quite similar for the resonances of the nucleobases in the interior part of these sequences, as evidenced by the resonance H6 of C8, for example. Exchange broadening of different resonances occurs at different temperatures, though, indicating that pre-melting dynamics depend on the length of the oligonucleotide.

If one were to deduce from experiments performed with and without fully complementary strands added to the immunostimulatory DNA[21,17] that the formation of Watson–Crick-paired helical regions does not occur, one might be misled. The presence of a fully complementary strand may suppress the formation of the structures observed here, and thus the presumed recognition by the receptor. In fact, it is likely that it will, as the stability of a full-length duplex will almost certainly be greater than that of the partial duplexes suggested here. A structure that is partly double-helical, but not a perfect duplex

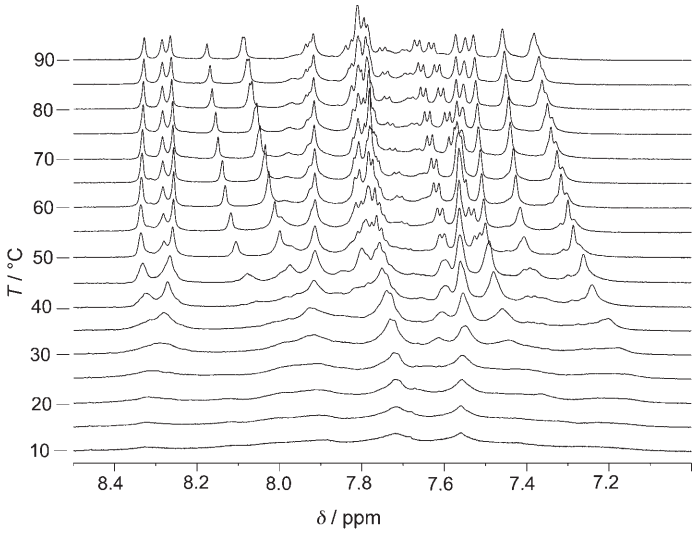

Figure 16. Thermal denaturation of the structure formed by pentaeicosamer **2**, as monitored by ^{1}H NMR spectra (downfield resonances) in the temperature range of 10–90 °C.

seems to be advantageous for activation of the innate immune system. This conclusion is consistent with the immunostimulatory activity of sequences that form partial duplexes studied by Agrawal and co-workers[53] and our own previous work favoring a model of recognition of partial duplexes.[36] Furthermore, a combination of established recognition motifs such as the methylation status of cytosines,[54] detectable in the major groove, with unusual structural features formed by other parts of the sequence may make selectivity easier to achieve.

An obvious question is whether the structure found is truly relevant. If the pattern-recognition receptors of the innate immune system arose to detect bacterial and/or viral DNA, then most likely they would have evolved to recognize DNA that was initially full-length double-stranded. Since it is known that TLR9 signaling occurs only after endocytosis,[51,52,55] it is likely that it starts after the initially double-stranded DNA has been digested into fragments similar to the synthetic oligonucleotides studied here. Further, the prevalence of CpG motifs in bacterial DNA make it likely that homo- and heteroduplexes can form between such fragments inside the endosomes. The concentration of relevant bacterial or synthetic DNA fragments that get sequestered into endosomes where TLR9 signaling occurs is not clear, but it is reasonable to assume that it is high enough for duplex formation to occur to a significant extent. To permit the calculation of melting points at various concentrations and percent duplex form at different temperatures, we have determined the enthalpy and entropy of duplex formation for eicosamer **1** and decamer **4** (Table 1).

The fact that the melting points of duplexes such as that of $(\mathbf{1})_2$ are slightly below body temperature does not mean that such duplexes are not recognized. A substantial portion of the DNA is in duplex form well above the midpoint of the melting transition. The transition, as detected by chemical shift changes, occurs up to rather high temperatures (compare Figures 8, 11, 14 and 16). Furthermore, and perhaps more importantly, the presence of a receptor that can bind such forms will necessarily shift the equilibrium towards the duplex form. Whereas binding a truly single-stranded DNA into a tight, well-ordered complex would most probably cost many kilocalories per mole (compare the enthalpic and entropic compensation associated with DNA duplex formation), binding a duplex should be much less entropically costly. Moreover, we previously demonstrated that methylation at N3 of thymidine residues, which disrupts Watson–Crick base pairing, massively decreases the immunostimulatory effect of the CpG oligonucleotide sequence studied herein.[36]

In conclusion, our data show that the well-established immunostimulatory sequence **1** forms duplex regions, and that structure formation also occurs in regions of the sequence that are outside the core hexamer GACGTT. It is unlikely that the nucleotides that engage in structure formation outside the core hexamer do so by simple Watson–Crick base pairing. Instead, it is more likely that they either fold back onto the core hexamer and/or form noncanonical structures remote from the core hexamer. The resulting three-dimensional structure may be unique enough to explain how the innate immune system manages to recognize synthetic CpG oligonucleotides (and bacterial DNA) against a possible background of host DNA set free through trauma, apoptosis, or other events that liberate host DNA inside the body. Recognition of an unusual three-dimensional structure rather than a smooth canonical duplex is likely, because the possible structural diversity is much greater if one takes noncanonical structures into account than it would be if one were to limit the repertoire to sequences of perfect duplexes. Thus, full three-dimensional structures of immunostimulatory sequences as well as structures of other immunostimulatory DNA[41,56] and RNA[57] sequences, let alone structures of complexes with Toll-like receptors are most desirable. Experiments to obtain such structures are currently underway in our research groups. Even in their absence, the structural information presented herein may affect the design of oligonucleotides with immunostimulatory activity that have therapeutic potential.[58] Needless to say, no one can claim to know the exact prerequisites for TLR9 recognition until a high-resolution three-dimensional structure of a complex with a ligand becomes available, and perhaps not even then.

Experimental Section

Sample preparation: All oligonucleotides employed were generated synthetically. The synthesis of hexamer **3** was reported previously.[37] Samples of decamer **4**, tetradecamer **5**, and eicosamer **1** were purchased in HPLC-purified form from Biospring (Frankfurt, Germany), whereas pentaeicosamer **2** was from Operon (Cologne, Germany). The samples were checked by mass spectrometry: **4**, MALDI-TOF MS for $C_{97}H_{124}N_{35}O_{59}P_9$ $[M-H]^-$ calcd 3002.0, found 3000.3; **5**, MALDI-TOF MS for $C_{135}H_{173}N_{48}O_{84}P_{13}$ $[M-H]^-$ calcd 4213.8, found 4212.6; **1**, MALDI-TOF MS for $C_{194}H_{248}N_{67}O_{122}P_{19}$ $[M-H]^-$ calcd 6057.9, found 6056.5; **2**, MALDI-TOF MS for $C_{244}H_{308}N_{92}O_{152}P_{24}$ $[M-H]^-$ calcd 7704.1, found 7707.7. Samples were lyophilized twice from D_2O. The residues were dissolved in D_2O containing NaCl (150 mM) and phosphate buffer (10 mM, pH 7 uncorrected for deuterium effect), with a final volume of ~180 μL.

The salts had been previously lyophilized from D_2O to decrease water content. For the acquisition of spectra detecting exchangeable protons, the samples were lyophilized to dryness and immediately taken up in H_2O/D_2O (9:1 *v/v*). The strand concentrations in the individual NMR solutions were as follows: **4**, 2 mM; **5**, 5.1 mM; **1**, 4.3 mM; **2**, 2.6 mM.

NMR spectroscopy: All NMR spectra were recorded in NMR microtubes susceptibility-matched to D_2O (Shigemi Co., Tokyo, Japan) on a Bruker AVANCE 600 spectrometer. Two-dimensional spectra were acquired with 4k–16k data points in f2 and 512 increments in f1. For samples in D_2O, suppression of the excess solvent peak was achieved by presaturation during the recycle delay. For samples in H_2O/D_2O (9:1 *v/v*), suppression was achieved by using the WATERGATE pulse sequence.[47] All NOESY spectra[59] were acquired with a mixing time of 250 ms. The DQF-COSY[60] and TOCSY[61] spectra were acquired to aid the assignment. The latter were run with a spin-lock time of 60 ms. Spectra were processed using XWINNMR (Bruker Biospin, Rheinstetten, Germany). A combination of exponential and Gaussian window functions was used during processing both dimensions. All spectra were calibrated to trimethylsilylpropionic acid at 0.0 ppm. Line widths of peaks (half-height peak width) were usually measured in one-dimensional spectra. For temperatures at which two-dimensional spectra were available, line widths of partially overlapping peaks were determined in slices of NOESY spectra. A full list of NMR spectra acquired is given in Table S1 of the Supporting Information.

Generation of low-resolution 3D structure of $(GACGTT)_2$: The preparation of the NMR sample of the hexamer in phosphate-buffered saline in D_2O has been reported previously.[37] One- and two-dimensional ^1H NMR spectra (NOESY, COSY, and TOCSY) were acquired at 600 MHz and 283 K. Peak assignment was also reported previously.[37] NOESY cross-peaks were integrated in a spectrum acquired at a mixing time of 250 ms using Sparky (version 3, available from Dr. T. D. Goddard and Dr. D. G. Kneller, University of California, San Francisco) and a Gaussian fit function. Integration values were converted into distance constraints based on a calibration function with the distances and cross-peak intensities of proton pairs with known distance, such as H5/H6 of cytosine. Typical boundaries for distance constraints were ± 1 Å. The available constraints, together with base-pairing constraints for the four canonical and the two wobble base pairs were then used to generate three-dimensional structures by using the torsion angle molecular dynamics option in CNS,[62] version 1.1. Distance constraints produced by a relaxation matrix approach in MARDIGRAS[63] or the isolated spin-pair approximation gave similar results. A total of 162 (2×81) constraints were used for generating the structures shown in Figure 3. Base-pair planarity constraints were set to a very modest value of nmr.plan.-scale = 15. The aligned overlay of the lowest-energy structures (Figure 3a) was generated in VMD.[64] The structure displaying the distance constraints (Figure 3b) was produced with a module operating in VMD that was written in-house.

Immunostimulatory activity: Custom-synthesized phosphorothioate-modified oligodeoxynucleotide 1668-PS was purchased from TIB MOLBIOL (Berlin, Germany). RAW 264.7 cells (a kind gift from Dr. R. Schumann, Berlin, Germany) were cultured in RPMI 1640 supplemented with 5% fetal calf serum (FCS), β-mercaptoethanol (50 μM), and antibiotics (penicillin G (100 IU mL^{-1} medium) and streptomycin sulfate (100 IU mL^{-1} medium). 1.5×10^5 cells per well were plated in 96-well culture plates and incubated with different oligodeoxynucleotides at the indicated concentrations. Where indicated, oligodeoxynucleotides were complexed with DOTAP (*N*-(2,3-dioleoyloxy-1-propyl)trimethylammonium methyl sulfate; Roth, Karlsruhe, Germany) as follows: oligodeoxynucleotides and DOTAP were diluted to a ratio of 1:5 in OPTIMEM (Invitrogen, Karlsruhe, Germany), incubated for 10 min at room temperature, and then added to the cells, which were cultured in RPMI/FCS medium without antibiotics. Supernatants were harvested for determination of cytokines after 24 h. Each cell-culture plate was stimulated with commercially available 1668-PS to control for inter-assay variation. Cytokine levels in culture supernatants were determined with commercially available ELISA kits for TNFα according to the manufacturer's instructions (BD Biosciences, Heidelberg, Germany). Measurements were done in duplicate.

Acknowledgements

The authors thank P. Lang, University of Karlsruhe, for the acquisition of some of the NMR spectra and C. Ahlborn, K. Gießler, S. Vogel, M. Printz, R. Eisenhuth, and C. Deck for a review of the manuscript. G.H. was a recipient of a fellowship from the State of Baden-Württemberg and Jiangsu Polytechnic University. This work was supported by the Landesstiftung Baden-Württemberg (project number P-LS-RNS/25) and DFG (He1452/5). The 600 MHz NMR facility at the University of Karlsruhe was supported by a grant from the Landesstiftung Baden-Württemberg.

Keywords: CpG oligonucleotides · DNA · immunostimulation · NMR spectroscopy · structure

[1] D. M. Klinman, *Nat. Rev. Immunol.* **2004**, *4*, 249–257.
[2] A. H. Dalpke, K. Heeg, *Int. J. Med. Microbiol.* **2004**, *294*, 345–354.
[3] S. Yamamoto, T. Yamamoto, S. Shimada, E. Kuramoto, O. Yano, T. Kataoka, T. Tokunaga, *Microbiol. Immunol.* **1992**, *36*, 983–997.
[4] E. Uhlmann, A. Peyman, *Chem. Rev.* **1990**, *90*, 543–584.
[5] H. Wagner, *Adv. Immunol.* **1999**, *73*, 329–368.
[6] T. Sparwasser, T. Miethke, G. B. Lipford, A. Erdmann, H. Häcker, K. Heeg, H. Wagner, *Eur. J. Immunol.* **1997**, *27*, 1671–1679.
[7] a) G. B. Lipford, M. Bauer, C. Blank, R. Reiter, H. Wagner, K. Heeg, *Eur. J. Immunol.* **1997**, *27*, 2340–2344; b) D. M. Klinman, *Expert Rev. Vaccines* **2003**, *2*, 305–315.
[8] A. M. Harandi, J. Sanchez, K. Eriksson, J. Holmgren, *Curr. Opin. Invest. Drugs* **2003**, *4*, 156–161.
[9] A. M. Krieg, *Nat. Rev. Drug Discovery* **2006**, *5*, 471–484.
[10] A. Dalpke, S. Zimmermann, K. Heeg, *BioDrugs* **2002**, *16*, 419–431.
[11] L. A. J. O'Neill, *Science* **2004**, *303*, 1481–1482.
[12] H. Wagner, *Trends Immunol.* **2004**, *25*, 381–386.
[13] G. M. Barton, R. Medzhitov, *Science* **2003**, *300*, 1524–1525.
[14] A.-M. Dragoi, X. Fu, S. Ivanov, P. Zhang, L. Sheng, D. Wu, G. C. Li, W.-M. Chu, *EMBO J.* **2005**, *24*, 779–789.
[15] H. Hemmi, O. Takeuchi, T. Kawai, T. Kaisho, S. Sato, H. Sanjo, M. Matsumoto, K. Hoshino, H. Wagner, K. Takeda, S. Akira, *Nature* **2000**, *408*, 740–745.
[16] S. Cornelie, J. Hoebeke, A. M. Schacht, B. Bertin, J. Vicogne, M. Capron, G. J. Riveau, *Biol. Chem.* **2004**, *279*, 15124–15129.
[17] M. Rutz, J. Metzger, T. Gellert, P. Luppa, G. B. Lipford, H. Wagner, S. Bauer, *Eur. J. Immunol.* **2004**, *34*, 2541–2550.
[18] J. Choe, M. S. Kelker, I. A. Wilson, *Science* **2005**, *309*, 581–585.
[19] J. K. Bell, I. Botos, P. R. Hall, J. Askins, J. Shiloach, D. M. Segal, D. R. Davies, *Proc. Natl. Acad. Sci. USA* **2005**, *102*, 10976–10980.
[20] N. J. Gay, M. Gangloff, A. N. R. Weber, *Nat. Rev. Immunol.* **2006**, *6*, 693–698.
[21] S. Zelenay, F. Elias, J. Flo, *Eur. J. Immunol.* **2003**, *33*, 1382–1392.
[22] See also: T. Tokunaga, O. Yano, E. Kuramoto, Y. Kimura, T. Yamamoto, T. Kataoka, S. Yamamoto, *Microbiol. Immunol.* **1992**, *36*, 55–66.
[23] P. Lenert, A. J. Goeken, R. F. Ashman, *Immunology* **2006**, *117*, 474–481.

[24] C. C. N. Wu, J. Lee, E. Ray, M. Corr, D. A. Carson, *J. Biol. Chem.* **2004**, *279*, 33071 – 33078.
[25] D. M. Klinman, A. K. Yi, S. L. Beaucage, J. Conover, A. M. Krieg, *Proc. Natl. Acad. Sci. USA* **1996**, *93*, 2879 – 2883.
[26] G. Hartmann, R. D. Weeratna, Z. K. Ballas, S. Payette, S. Blackwell, I. Suparto, W. L. Rasmussen, D. Waldschmidt, D. Sajuthi, R. H. Purcell, H. L. Davis, A. M. Krieg, *J. Immunol.* **2000**, *164*, 1617 – 1624.
[27] E. R. Kandimalla, L. Bhagat, D. Yu, Y. P. Cong, J. Tang, S. Agrawal, *Bioconjugate Chem.* **2002**, *13*, 966 – 974.
[28] D. Yu, E. R. Kandimalla, L. Bhagat, J. Y. Tang, Y. P. Cong, J. Tang, S. Agrawal, *Nucleic Acids Res.* **2002**, *30*, 4460 – 4469.
[29] Y. Li, E. R. Kandimalla, D. Yu, S. Agrawal, *Int. Immunopharmacol.* **2005**, *5*, 981 – 991.
[30] R. A. Goldsby, T. J. Kindt, B. A. Osborne, J. Kuby, *Immunology*, 5th ed., W. H. Freeman, New York, **2002**, pp. 69 – 72.
[31] See for example: J. G. Arnez, T. A. Steitz, *Biochemistry* **1996**, *35*, 14725 – 14733.
[32] N. D. Clarke, J. M. Berg, *Science* **1998**, *282*, 2018 – 2022.
[33] W. Saenger, *Principles of Nucleic Acid Structure*, Springer, New York, **1984**, pp. 137 – 140.
[34] Y. Choo, A. Klug, *Curr. Opin. Struct. Biol.* **1997**, *7*, 117 – 125.
[35] a) A. M. Krieg, S. M. Efler, M. Wittpoth, J. Al Adhami, H. L. Davis, *J. Immunother.* **2004**, *27*, 460 – 471; b) J. Vollmer, *Expert Opin. Biol. Ther.* **2005**, *5*, 673 – 682.
[36] J. Vollmer, *Int. Rev. Immunol.* **2006**, *25*, 125 – 134.
[37] S. Narayanan, A. H. Dalpke, K. H. Siegmund, K. Heeg, C. Richert, *J. Med. Chem.* **2003**, *46*, 5031 – 5044.
[38] E. R. Kandimalla, L. Bhagat, Y. Li, D. Yu, D. Wang, Y.-P. Cong, S. S. Song, J. X. Tang, T. Sullivan, S. Agrawal, *Proc. Natl. Acad. Sci. USA* **2005**, *102*, 6925 – 6930.
[39] A. M. Krieg, Y. Ae-Kyung, S. Matson, T. J. Waldschmidt, G. A. Bishop, R. Teasdale, G. A. Koretzky, D. M. Klinman, *Nature* **1995**, *374*, 546 – 549.
[40] a) S. W. Lee, M. K. Song, K. H. Baek, Y. Park, J. K. Kim, C. H. Lee, H. K. Cheong, C. Cheong, Y. C Sung, *J. Immunol.* **2000**, *165*, 3631 – 3639; b) A. H. Dalpke, S. Zimmermann, I. Albrecht, K. Heeg, *Immunology* **2002**, *106*, 102 – 112; c) H. Bartz, Y. Mendoza, M. Gebker, T. Fischborn, K. Heeg, A. Dalpke, *Vaccine* **2004**, *23*, 148 – 155; d) Z. Zhang, U. Fauser, H. J. Schluesener, *Neuroreport* **2006**, *17*, 1579 – 1583.
[41] a) D. Verthelyi, K. J. Ishii, M. Gursel, F. Takeshita, D. M. Klinman, *J. Immunol.* **2001**, *166*, 2372 – 2377; b) J. D. Marshall, E. M. Hessel, J. Gregorio, C. Abbate, P. Yee, M. Chu, G. Van Nest, R. L. Coffman, K. L. Fearon, *Nucleic Acids Res.* **2003**, *31*, 5122 – 5133.
[42] D. J. Patel, S. A. Kozlowski, L. A. Marky, C. Broka, J. A. Rice, K. Itakura, K. J. Breslauer, *Biochemistry* **1982**, *21*, 428 – 436.
[43] D. J. Patel, L. L. Canuel, *Eur. J. Biochem.* **1979**, *96*, 267 – 276.
[44] For related use of this transfection agent, see for example: K. Yasuda, P. Yu, C. J. Kirschning, B. Schlatter, F. Schmitz, A. Heit, S. Bauer, H. Hochrein, H. Wagner, *J. Immunol.* **2005**, *174*, 6129 – 6136.
[45] G. M. Barton, J. C. Kagan, R. Medzhitov, *Nat. Immunol.* **2006**, *7*, 49 – 56.
[46] S. S. Wijmenga, M. M. W. Mooren, C. W. Hilbers, *NMR of Macromolecules: A Practical Approach* (Ed.: G. C. K. Roberts), Oxford University Press, Oxford, **1993**. pp. 217 – 288.
[47] V. Sklenar, M. Piotto, R. Leppik, V. Saudek, *J. Magn. Reson. Ser. A* **1993**, *102*, 241 – 245.
[48] J. A. McDowell, D. H. Turner, *Biochemistry* **1996**, *35*, 14077 – 14089.
[49] a) I. G. Panyutin, O. I. Kovalsky, E. I. Buddowsky, R. E. Dickerson, M. E. Rikhirev, A. A. Lipanov, *Proc. Natl. Acad. Sci. USA* **1990**, *87*, 867 – 870; b) Y. Wang, D. J. Patel, *J. Mol. Biol.* **1993**, *234*, 1171 – 1183; c) G. N. Parkinson, M. P. H. Lee, S. Neidle, *Nature* **2002**, *417*, 876 – 880; d) J. T. Davis, *Angew. Chem.* **2004**, *116*, 684 – 716; *Angew. Chem. Int. Ed.* **2004**, *43*, 668 – 698; e) A. T. Phan, V. Kuryavyi, D. J. Patel, *Curr. Opin. Struct. Biol.* **2006**, *16*, 288 – 298.
[50] C. Guiducci, G. Ott, J. H. Chan, E. Damon, C. Calacsan, T. Matray, K.-D. Lee, R. L. Coffman, F. J. Barrat, *J. Exp. Med.* **2006**, *203*, 1999 – 2008.
[51] H. Häcker, H. Mischak, T. Miethke, S. Liptay, R. Schmid, T. Sparwasser, K. Heeg, G. B. Lipford, H. Wagner, *EMBO J.* **1998**, *17*, 6230 – 6240.
[52] K. Yasuda, Y. Ogawa, I. Yamane, M. Nishikawa, Y. Takakura, *J. Leukocyte Biol.* **2005**, *77*, 71 – 79.
[53] E. R. Kandimalla, L. Bhagat, Y.-P. Cong, R. K. Pandey, D. Yu, Q. Zhao, S. Agrawal, *Biochem. Biophys. Res. Commun.* **2003**, *306*, 948 – 953.
[54] See for example: a) K. Kariko, M. Buckstein, H. Ni, D. Weissman, *Immunity* **2005**, *23*, 165 – 175; b) I. Ohki, N. Shimotake, N. Fujita, J.-G. Jee, T. Ikegami, M. Nakao, M. Shirkawa, *Cell* **2001**, *105*, 487 – 497; c) N. M. Inamdar, K. C. Ehrlich, M. Ehrlich, *Plant Mol. Biol.* **1991**, *17*, 111 – 123.
[55] K. J. Stacey, M. Sweet, D. A. Hume, *J. Immunol.* **1996**, *157*, 2116 – 2122.
[56] M. Jurk, A. Kritzler, H. Debelak, J. Vollmer, A. M. Krieg, E. Uhlmann, *ChemMedChem* **2006**, *1*, 1007 – 1014.
[57] A. D. Judge, V. Sood, J. R. Shaw, D. Fang, K. McClintock, I. MacLachlan, *Nat. Biotechnol.* **2005**, *23*, 457 – 462.
[58] I. Wickelgren, *Science* **2006**, *312*, 184 – 187.
[59] A. Kumar, R. R. Ernst, K. A. Wüthrich, *Biochem. Biophys. Res. Commun.* **1980**, *95*, 1 – 6.
[60] U. Piantini, O. W. Sørensen, R. R. Ernst, *J. Am. Chem. Soc.* **1982**, *104*, 6800 – 6801.
[61] A. Bax, D. Davis, *J. Magn. Reson.* **1985**, *65*, 355 – 360.
[62] A. T. Brünger, P. D. Adams, G. M. Clore, W. L. DeLano, P. Gros, R. W. Grosse-Kunstleve, J. S. Jiang, J. Kuszewski, M. Nilges, N. S. Pannu, R. J. Read, L. M. Rice, T. Simonson, G. L. Warren, *Acta Crystallogr. Sect. D* **1998**, *54*, 905 – 921.
[63] B. A. Borgias, T. L. James, *J. Magn. Reson.* **1990**, *87*, 475 – 487.
[64] W. Humphrey, A. Dalke, K. Schulten, *J. Mol. Graphics* **1996**, *14*, 33 – 38.

Received: November 8, 2006
Revised: December 22, 2006
Published online on March 16, 2007

